ISSN 1392-1320 MATERIALS SCIENCE (MEDŽIAGOTYRA). Vol. XX, No. X. 2026

The Effect of Sc on the Biocorrosion Properties of Selected Zinc-Based Biomaterials

Salem A G SALEH, İsmail Hakkı KARA *

Metallurgy and Materials Engineering Department of Engineering Faculty, Karabük University, Karabük,78050, Turkey

http://doi.org/10.5755/j02.ms.41282

Received 23 April 2025; accepted 12 June 2025

In this study, Zn-based alloys were produced by the conventional casting technique. After homogenization heat treatment, microstructural properties and corrosion life of pure zinc, Zn-Mg, Zn-Mg-Al, and Zn-Mg-Al-Sc alloys were investigated. Effects of additional elements, heat treatment, and phases formed in the structures affecting corrosion resistance were systematically investigated. To evaluate corrosion, we performed electrochemical and immersion tests in Hank's salt solution. Corrosion resistance deteriorated in scandium-added Zn-Mg-Al-Sc alloys due to localized galvanic coupling, whereas we observed improvements in microstructure. On a positive note, the Zn-Mg-Al alloy showed the best corrosion resistance. Our findings on the microstructural changes and corrosion resistance effects of Sc addition to biodegradable Zn-based alloys helped to explain the complex role played by Sc. The previous studies focused mostly on binary and ternary systems of Zn alloys. However, new insight into the role of Sc adding in Zn-based alloys is contributed by this study. The findings of our study clarify the effect of Sc on the microstructure and bio-corrosion behavior of Zn-based alloys. As a result, more reliable biodegradable Zn-based alloys will be designed thanks to this study.
Keywords: zinc-based alloys, scandium, heat treatment, biocorrosion.

1. INTRODUCTION

Zinc alloys are promising materials for biomedical implants due to their natural dissolution ability. However, the rapid degradation of pure zinc leads to the release of cytotoxic Zn^{2+} ion concentrations that can be harmful to body tissues. The alloying elements magnesium (Mg), aluminum (Al), and scandium (Sc) are employed to enhance both mechanical and corrosion properties. The lack of consensus in studies concerning the biodegradation behavior of the Sc element, which is known to be advantageous regarding mechanical properties, calls for further investigations on this topic [1 – 3].

The main benefits of scandium to zinc alloys can be summarized as follows: scandium promotes microstructural refinement, resulting in a finer and more uniform grain structure; scandium contributes to increased hardness and tensile strength, increasing the load-carrying capacity of the alloy under mechanical stress [4, 5].

In the literature, it is invesitgated on elucidating the role of scandium in regulating alloy performance in the Zn-3Cu-0.4Li-xSc system. The researchers have shown that a high scandium concentration contributes to improved corrosion resistance. The optimum scandium content was determined to be 0.5 wt.% alloy, and this content was reported to provide the most effective protection against corrosion. In addition, the presence of the intermetallic phase $ScZn_{12}$ was associated with high cellular compatibility, robust osteogenic stimulation, and anti-inflammatory activity [6].

Moreover it is developed the Zn-4Ag-0.1Sc alloy for use in guided bone regeneration (GBR) membrane applications. Both in vitro and in vivo evaluations were performed to investigate the mechanical performance, biocompatibility, osteogenic capacity, and antibacterial properties of the alloy. The addition of silver and scandium contributed to the improvement of mechanical strength and corrosion control and promoted cytocompatibility, osteogenic differentiation, and anti-infection behavior. [7].

The designed Zn-4Ag-0.1Sc alloy is a candidate alloy for biodegradable implant applications, especially in orthopedic contexts, due to its synergistic combination of biocompatibility, antibacterial activity, and osteogenic potential. In vitro studies have shown significant antibacterial activity against both Staphylococcus aureus and Escherichia coli in reducing the risk of infection associated with implantable devices. Furthermore, in vivo evaluations have confirmed that the alloy promotes bone regeneration by stimulating osteogenic activity [5].

In the present study, a series of zinc-based alloys were systematically developed by adding magnesium (Mg), aluminum (Al), and scandium (Sc). The alloys were produced by conventional gravity casting with precise control over the chemical composition to elucidate the specific roles of Mg, Al, and Sc in enhancing the corrosion resistance of the Zn matrix. Scanning electron microscopy (SEM) and X-ray diffraction (XRD) were used to evaluate the microstructural features of the alloys. A comprehensive corrosion testing technique consisting of electrochemical and immersion tests was employed. The findings from this study are intended to contribute to the advancement of high-performance zinc-based materials for potential use in biomedical implants.

* Corresponding author: İ.H. Kara
E-mail: *ihakkikara@karabuk.edu.tr*

2. EXPERIMENTAL DETAILS

A conventional gravity casting technique was used to produce experimental zinc-based materials. Pure zinc ingots were placed in an electric resistance furnace preheated to 600 °C. Pure magnesium and aluminum were then added, and the furnace temperature was increased to 700 °C. Al-Sc master alloy was added to the furnace, and the molten mixture was stirred at 700 °C for 10 min to ensure homogeneity. The casting temperature was maintained at 600 °C, and the molten alloys were poured into a steel mold kept at room temperature (25 °C). The chemical compositions of the produced alloys were analysed using a spectrometer, and the results are given in Table 1.

Table 1. Chemical composition of zinc-based alloys

Materials	No	Mg	Al	Sc	Zn
Pure Zn	1	–	–	–	bal.
Zn-Mg	2	0.55	–	–	bal.
Zn-Mg-Al	3	0.53	0.42	–	bal.
Zn-Mg-Al-Sc	4	0.49	0.42	0.50	bal.

In addition, the samples were subjected to a homogenization heat treatment at 300 °C for 4 h. Carl Zeiss Ultra Plus scanning electron microscopy (SEM) equipped with an energy dispersive x-ray spectroscopy (EDX) and X-ray diffractometer (Rigaku ULTIMA IV) was used for microstructural characterization. ImageJ software was used to calculate average grain size. Biocorrosion behavior was evaluated using the potentiodynamic polarization method according to ASTM G102-89 (2004). The open circuit potential (OCP) stabilization time was set at 300 s, and the scan rate was 1.5 mV/s. A silver/silver chloride (Ag/AgCl) electrode was used as the reference, and graphite rods were used as the counter electrode. Hank's solution was used as the electrolyte medium. Corrosion tests were carried out at a controlled temperature of 37.5 ± 0.5 °C. Moreover, immersion corrosion tests were carried out to support the potentiodynamic corrosion tests in Hank‘s solution during seven days at 37.5 ± 0.5 °C.

3. RESULTS AND DISCUSSION

3.1. Microstructure

SEM results indicate that scandium-containing alloys exhibited significantly refined grain morphologies and dual-phase microstructures, suggesting a grain refining effect by Sc (see Fig. 1). As to the grain sizes of samples, sample 1 has a lamellar structure, and the grain boundaries are not clear to calculation. However, samples 2, 3, and 4 impart clear grains. As for samples 2, 3, and 4, the average grain sizes are 2.5 ± 0.5 μm, 1.25 ± 0.25 μm, and 1.75 ± 0.25 μm.

XRD patterns reveal the formation of multiple phases, including the Zn phase and intermetallic compounds such as $Zn_{11}Mg_2$, $MgZn_2$, and Zn-Al-based phases. The addition of scandium resulted in the production of Sc-containing intermetallic compounds called ScZn and Sc_2Zn_{17} (see Fig. 2).

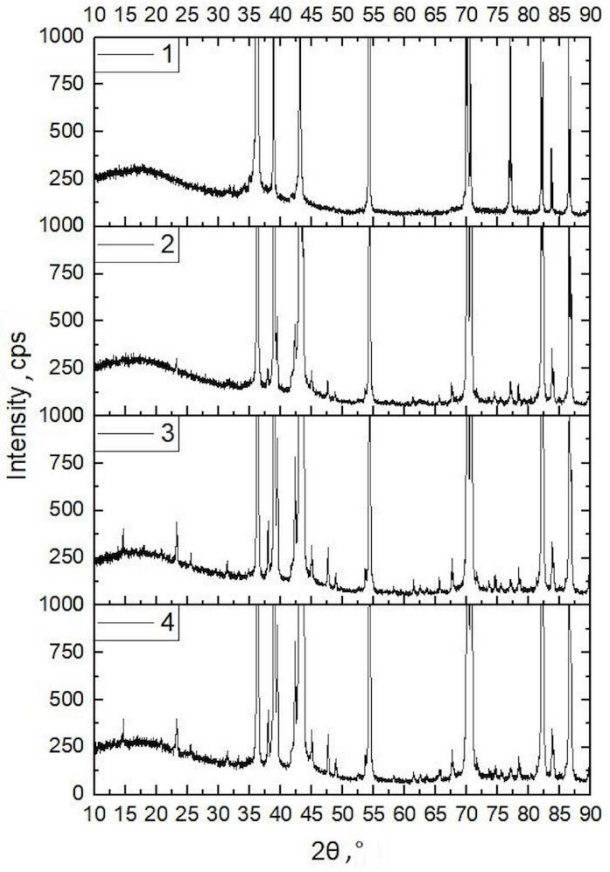

Fig. 2. X-ray diffraction (XRD) patterns of samples 1, 2, 3, and 4 in the 2θ range of 10° – 90°

3.2. Phase distribution

To determine the distribution of phases, phase quantification was performed using volume, mass, and mole fractions. Sample 1, which was made of pure zinc, showed no discernible secondary phase, and the microstructure consisted mainly of hexagonal close-packed (hcp) Zn phase.

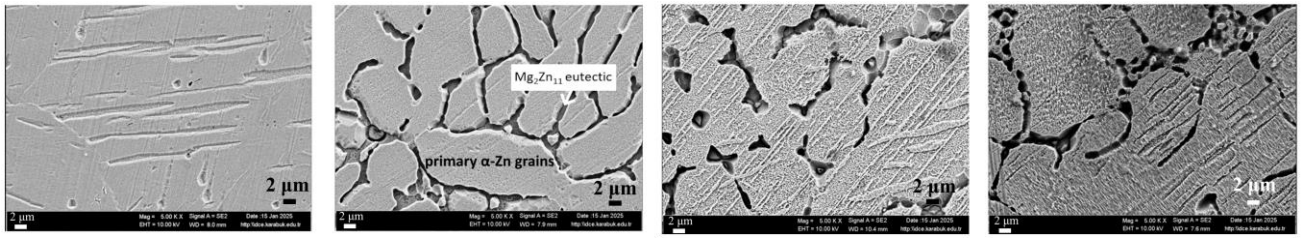

a b c d

Fig. 1. SEM images of samples: a – 1; b – 2; c – 3; d – 4

Zn and $Zn_{11}Mg_2$ secondary phases were roughly equally distributed in volume in Sample 4 (Zn-Mg-Al-Sc). Additionally, trace amounts of zinc oxide (ZnO) were found, which was formed because of exposure to ambient conditions.

3.3. Corrosion behavior

Electrochemical tests show that there are significant differences in the corrosion behavior of Zn-based alloys (see Table 2). Among all alloys, Zn-Mg-Al alloy exhibited the highest corrosion resistance (0.017 mm/year), while Zn-Mg-Al-Sc alloy exhibited the highest corrosion rate (0.56 mm/year). There was a significant decrease in corrosion resistance with the addition of scandium. The most positive E_{corr} value was observed for Zn-Mg-Al alloy, whereas the most negative E_{corr} value was observed for pure Zn. Consistent with the superior resistance to corrosion of Zn-Mg-Al alloy, it reflects its natural susceptibility to corrosion in physiological environments [7].

The addition of Mg shifted E_{corr} to a more positive direction, and this positively affected the corrosion resistance. Further improvement was achieved with the addition of Al, resulting in a higher oxidation potential, which contributed to the formation of a protective surface layer. However, the inclusion of scandium in the Zn-Mg-Al system caused a negative shift in Ecorr and promoted localized galvanic corrosion. It is known that the formation of galvanic microcells between the Zn matrix and secondary phases such as $Mg_2(Zn, Al)_{11}$ causes this result [5].

Table 2. Corrosion results of potentiodynamic tests

No.	Cathodic slope	Anodic slope	CC, μA	CCD, μA/cm^2	CR, mm/year	Ecorr, V
1	-0.51	0.013	1.56	14.58	0.22	-1.67
2	-0.224	0.0010	1.87	17.48	0.26	-1.13
3	-0.393	0.192	0.12	1.12	0.017	-0.34
4	-0.072	0.005	3.97	37.1	0.56	-1

Fig. 3 presents the comparative analysis of the polarization curves for Samples 1 to 4.

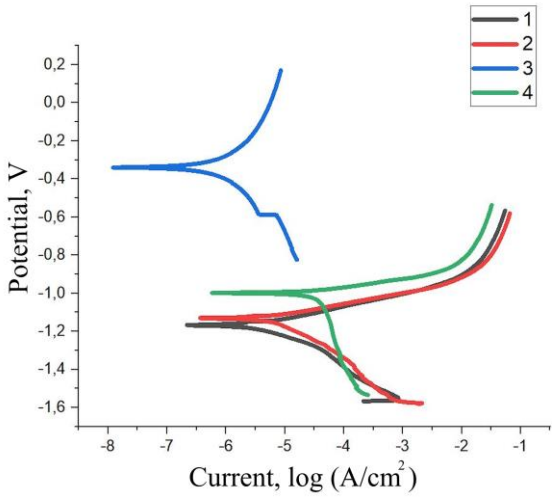

Fig. 3. Tafel curves of specimens

Examination of the anodic branches shows that the corrosion processes in all samples are predominantly activation-controlled. This is evidence that the anodic dissolution of zinc is governed by charge transfer mechanisms rather than diffusion. In particular, the cathodic polarization behavior of Sample 4 deviates from this trend, exhibiting the characteristic features of diffusion-limited kinetics. This is evidenced by the vertically sloped cathodic branch of the polarization curve, which may be indicative of limited mass transport during the reduction reaction. The cathodic Tafel slope calculated for Sample 4 (0.072 V/decade) supports this situation and reflects a significant diffusion effect on the cathodic process in the presence of scandium-containing phases.

In contrast, Sample 4 showed the highest corrosion rate and corresponding corrosion current density (I_{corr}), indicating a significantly higher sensitivity to electrochemical degradation [4]. These findings suggest that the alloy arrangement of Sample 3 was more successful in stabilizing the Zn matrix and mitigating corrosion processes, whereas the microstructural or compositional features of Sample 4 were likely to enhance localized corrosion activity (see Fig. 4).

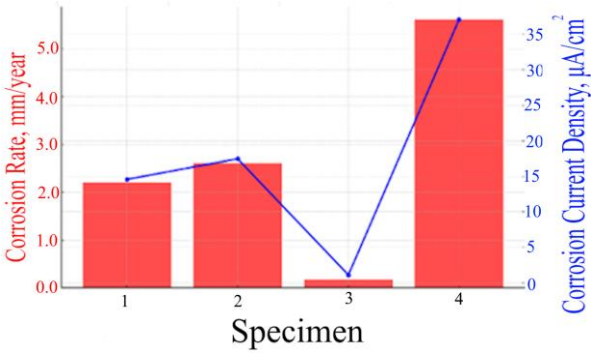

Fig. 4. Average daily change rates for each specimen

The immersion corrosion test shows us the significant progression trends in the corrosion behavior of the samples that adhered in the 1 – 4 and 4 – 7th day intervals. There is a minimal change for Sample 1 in both time periods. In other words, we see a stable change. Samples 2 and 4 showed significant increases, especially in the 4 – 7 day interval. This is due to a reason related to the degradation mechanisms. When we look at Sample 3, we see that there is an average and consistent change (see Fig. 5).

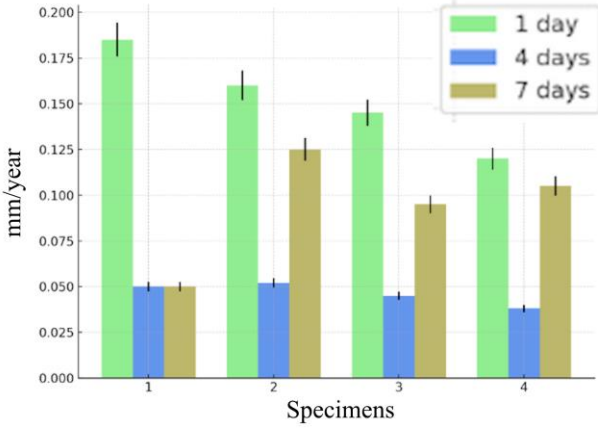

Fig. 5. The immersion corrosion results of specimens

EDX analysis results from three different regions of Sample 1 are given in Table 3.

Table 3. EDX results of samples taken in Fig. 6 are marked with spectrum numbers

Sample	Spectrum	O, mass %	Zn, mass %	Al, mass %	Mg, mass %	Sc, mass %
1	1	81.39	18.61	–	–	–
	2	97.02	2.98	–	–	–
	3	78.17	21.83	–	–	–
2	1	72.14	25.21	–	2.65	–
	2	71.30	22.04	–	6.67	–
	3	85.66	4.80	–	9.54	–
	4	69.13	15.44	–	15.43	–
3	1	64.99	24.55	10.47	0.00	–
	2	77.98	7.57	14.45	0.00	–
	3	71.77	12.07	14.00	2.16	–
	4	68.00	18.43	13.07	0.51	–
	5	80.85	12.24	6.91	0.00	–
4	1	64.25	8.11	25.54	0.00	2.10
	2	56.07	6.85	33.27	3.81	0.00
	3	70.14	14.98	11.38	0.69	2.81
	4	16.15	70.82	3.93	0.00	9.10
	5	72.80	13.95	9.33	0.00	3.92

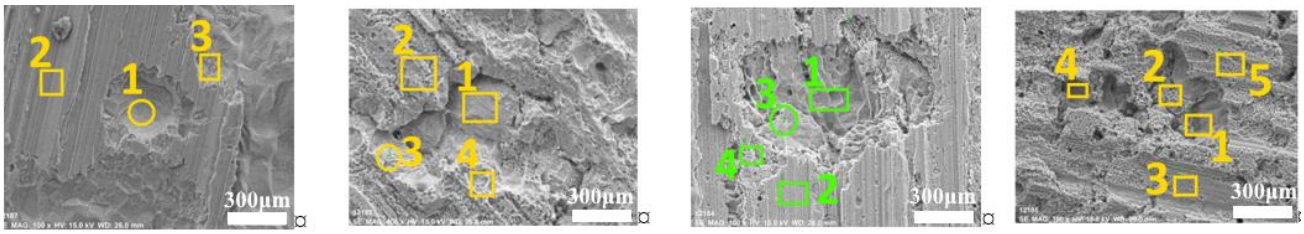

a b c d

Fig. 6. EDX and surface analysis of corroded samples: a – 1; b – 2; c – 3; d – 4

The high oxygen content here attracted our attention. The average oxygen concentration calculated as 85.53 % shows us the compositional heterogeneity on the deteriorated surface. The presence of almost pure oxide phases, probably ZnO or MgO, coincides with the results of Spectrum 2. It is known that MgO has a higher band gap and is less conductive than ZnO, which results in a decrease in the cathodic reaction during the corrosion process [8].

It can be said that partial passivation of the surface during corrosion occurs due to the development of the oxide layer [9]. This may be due to the formation of a coating by corrosion products or the disintegration of metallic zinc due to the decreasing zinc content. Here we can see the irregular corrosion that can be caused by uneven element distributions, irregular cooling during solidification or microsegregation. It also gives credibility to the theory that oxidation is facilitated by galvanic contacts between the $Zn_{11}Mg_2$ secondary phase and the Zn matrix [10]. Surface examination, which may be the cause of localized corrosion, shows significant surface deterioration characterized by widespread oxidation and various morphologies in the post-corrosion images of Sample 2. Here again, the acceleration of corrosion by localized attacks is due to micro-galvanic interaction [11].

The EDX results gave the following data for two different areas: Spectra 1 and 2 were 72.14 % O, 2.65 % Mg and 25.21 % Zn, 71.30 % O, 6.67 % Mg and 22.04 % Zn, 85.66 % O, 9.54 % Mg and 4.80 % Zn and 69.13 % O, 15.43 % Mg and 15.44 % Zn, respectively. Again, the presence of a thick corrosion product layer consisting of ZnO and MgO was evidenced [12]. Spectrum 3 showed almost complete surface oxidation in isolated areas containing more than 85 % oxygen and less than 5 % zinc.

As corrosion progresses, the formation of Mg-rich intermetallic phases or selective leaching of Zn may have led to higher magnesium content in some areas. This demonstrates the irregular corrosion in Sample 2 and the importance of microstructural features in influencing local corrosion behavior [13]. The corroded surface of Sample 3 shows us an irregular and distinct distribution originating from local corrosion events. We can again talk about micro-galvanic interactions as the mechanism. From the EDX results of Sample 3, the computed mean elemental composition for all locations was 72.72 % O, 0.53 % Mg, 11.78 % Al, and 14.97 % Zn. The moderate standard deviations, especially in the oxygen and zinc levels, showed that the corrosion on the surface was heterogeneous. The oxide layers consisting of ZnO and AlO_3 indicate oxygen-induced oxidation, and the almost complete absence of magnesium content indicates the preferred dissolution of Mg during corrosion [14]. It can be said that increasing oxygen values help the formation of a protective layer that will facilitate local passivation of aluminum.

The surface results after corrosion of Sample 4 show chemical heterogeneity and irregular oxide layer development. This is important to understand the reason for irregular corrosion behavior because the high standard deviations in zinc and oxygen levels indicate a heterogeneous corrosion process of the alloy surface. In addition, the constituent elements with different electrochemical potentials of the complex multiphase microstructure Zn-Mg-Al-Sc alloy contributed to local

degradation. Micro galvanic interactions are characterized by the simultaneous presence of passivated patches and local film degradation. A significant oxide layer consisting of ZnO, AlO_3, and probably ScO_3 has formed in most regions due to the dominance of oxygen [15]. The persistently high aluminium concentration indicates the presence of a passive aluminium protective coating. Local film degradation or reduced electrochemical activity indicates a region of lack of passivation due to the high zinc (70.82 %) and low oxygen (16.15 %) concentration of Spectrum 4. It can be said that the effect of Scandium on passive film stability may be probable from its presence in Spectra 1, 3, 4, and 5. However, non-uniform distribution may have been a factor in micro-galvanic effects and spatially varying corrosion resistance [16].

4. CONCLUSIONS

The Zn-Mg-Al alloy showed the best corrosion resistance, with the lowest corrosion rate (0.017 mm/yr) and the largest positive corrosion potential (E_{corr}). The addition of scandium to the Zn-Mg-Al combination resulted in a significant decrease in corrosion resistance, as indicated by a significantly higher corrosion rate (0.56 mm/yr) and a trend toward more negative Ecorr values. The loss in performance is due to galvanic interactions between the Zn matrix and intermetallic phases such as $Mg_2(Zn,Al)_{11}$, which promote localized corrosion.

REFERENCES

1. **Li, H., Zheng, Y., Qin, L.** Progress and Prospects in Biodegradable Metals for Biomedical Applications *Acta Biomaterialia* 10 (9) 2014: pp. 4561 – 4573. https://doi.org/10.1016/j.actbio.2014.07.005
2. **Yang, H., Wang, C., Liu, C., Chen, H., Wu, Y., Han, J., Jia, Z., Lin, W., Zhang, D., Li, W., Yuan, W., Guo, H., Li, H., Yang, G., Kong, D., Zhu, D., Takashima, K., Ruan, L., Nie, J., Li, X., Zheng, Y.** Evolution of The Degradation Mechanism of Pure Zinc Stent in The One-Year Study of Porcine Coronary Artery *Acta Biomaterialia* 60 2017: pp. 68 – 81. https://doi.org/10.1016/j.actbio.2017.07.020
3. **Franklin, N.M., Rogers, N.J., Apte, S.C., Batley, G.E., Gadd, G.E., Casey, P.S.** Comparative Toxicity of Nanoparticulate ZnO, Bulk ZnO, and $ZnCl_2$ to a Freshwater Microalga (Pseudokirchneriella subcapitata): The Importance of Particle Solubility *Environmental Science & Technology* 41 (24) 2007: pp. 8484 – 8490. https://doi.org/10.1021/es071445r
4. **Zhang, Y., Cheng, X., Wang, J., Liu, Z.** Effect of Scandium Addition on Mechanical Properties and Corrosion Resistance of Medium Strength Al-Zn-Mg-Cu Alloy *Materials Science Forum* 794 – 796 2023: pp. 241 – 246. https://doi.org/10.4028/www.scientific.net/MSF.794-96.241
5. **Liu, J., Zhang, X., Li, Y., Wang, Y., Chen, Q., Zhao, Y., Zhang, T., Liu, Y., Zhang, Y., Wang, L.** Biodegradable Zn–4Ag–0.1Sc Alloy with Enhanced Antibacterial and Osteogenic Properties *Chemical Engineering Journal* 490 2024: pp. 149834. https://doi.org/10.1016/j.cej.2024.149834
6. **Kabir, H., Lin, J., Munir, K.S., Wen, C., Wright, P., Li, Y.** Influence of Scandium on Mechanical Properties, Degradation Behavior, and Cytocompatibility of Zn–3Cu–0.4Li–xSc Alloys for Implant Applications *Materialia* 28 2023: pp. 101768. https://doi.org/10.1016/j.mtla.2023.101768
7. **Tong, X., Shen, X., Lin, Z., Lu, L., Munir, K., Zhou, R., Zhu, L., Li, Y., Ma, J., Wen, C., Lin, J.** In Vitro and In Vivo Studies of a Biodegradable Zn-4Ag-0.1Sc Alloy with High Strength–Elongation Product, Cytocompatibility, Osteogenic Differentiation, and Anti-Infection Properties for Guided Bone-Regeneration Membrane Applications *Chemical Engineering Journal* 493 2024: pp. 152763. https://doi.org/10.1016/j.cej.2024.152763
8. **Yao, C., Wang, Z., Tay, S.L., Zhu, T., Gao, W.** Effects of Mg on Microstructure and Corrosion Properties of Zn–Mg Alloy *Journal of Alloys and Compounds* 602 2014: pp. 101 – 107. https://doi.org/10.1016/j.jallcom.2014.03.025
9. **Xiang, E., Gómez-Cerezo, M.N., Ali, Y., Ramachandra, S.S., Yang, N., Dargusch, M., Abdal-Hay, A.** Surface Modification of Pure Zinc by Acid Etching: Accelerating the Corrosion Rate and Enhancing Biocompatibility and Antibacterial Characteristics *Applied Materials & Interfaces* 14 (19) 2022: pp. 22554 – 22569. https://doi.org/10.1021/acsami.2c03945
10. **Alaneme, K.K., Adediran, M.** Mechanical Behaviour and Bio-Corrosion Performance of Zn–Cu–Mn Based Alloys for Biomedical Applications *Manufacturing Review* 12 (8) 2025: pp. 01 – 10.
11. **Mozaffari, F., Salehi, M., Shabestari, S.G.** Microstructure, Mechanical Properties and Bio-Corrosion Behavior of Mg–2Zn–0.3Ca–x (x = 0, 0.5, 1.0) Y Alloys *Journal of Materials Research and Technology* 31 2024: pp. 1017 – 1027.
12. **Sun, X., Yu, X., Li, W., Chen, M., Liu, D.** Mechanical Properties, Degradation Behavior and Cytocompatibility of Biodegradable 3 vol% X (X = MgO, ZnO and CuO)/Zn Matrix Composites with Excellent Dispersion Property Fabricated by Graphene Oxide-Assisted Hetero-Aggregation *Biomaterials Advances* 134 2022: pp. 112722. https://doi.org/10.1016/j.msec.2022.112722
13. **Pulido-González, N., Hidalgo-Manrique, P., García-Rodríguez, S., Torres, B., Rams, J.** Effect of Heat Treatment on the Mechanical and Biocorrosion Behaviour of Two Mg–Zn–Ca Alloys *Journal of Magnesium and Alloys* 10 (2) 2022: pp. 540 – 554. https://doi.org/10.1016/j.jma.2021.06.022
14. **Miao, M., Zhao, S.R., Li, T., Liu, J.K., Liu, J.C., Liu, Z.X., Ma, Y.S., Zou, X.** In-Situ Synthesis and Excellent Corrosion Performance of Strontium Hydroxyphosphate/Polyaniline Composite with Wrapped *Structure Progress in Organic Coatings* 194 2024: pp. 108542. https://doi.org/10.1016/j.porgcoat.2024.108542
15. **Yang, L., Feng, Y., He, Y., Yang, L., Liu, H., Wang, X., Peng, C., Wang, R.** Effect of Sc/Sm Microalloying on Microstructural and Properties of Mg-2Zn-0.3Ca Biodegradable Alloy *Journal of Alloys and Compounds* 907 2022: pp. 164533. https://doi.org/10.1016/j.jallcom.2022.164533
16. **Ramanathan, P., Srinivasan, R., Neelakandan, S.** Third-Generation Biodegradable Bone Implants: A Novel Mg-1Zn-0.5Sc Alloy Treated by Laser Shock Peening to Improve Its Characteristics *Proceedings of the Institution of Mechanical Engineers, Part L,* 238 (2) 2023: pp. 225 – 244. https://doi.org/10.1177/14644207231206067